AFAL-TR-88-102 AD:

Fiber Optic Sensor System

Final Report
for the period
30 May 1986 to
1 June 1988

AD-A206 636

March 1989

Author:
J. S. Schoenwald

Rockwell International Science Center
1049 Camino Dos Rios
Thousand Oaks CA 91360

SC5463.FRD
F04611-86-C-0036

Approved for Public Release

Prepared for the: **Air Force Astronautics Laboratory**

Air Force Space Technology Center
Space Division, Air Force Systems Command
Edwards Air Force Base,
California 93523-5000

NOTICE

When U.S. Government drawings, specifications, or other data are used for any purpose other than a definitely related Government procurement operation, the fact that the Government may have formulated, furnished, or in any way supplied the said drawings, specifications, or other data, is not to be regarded by implication or otherwise, or in any way licensing the holder or any other person or corporation, or conveying any rights or permission to manufacture, use, or sell any patented invention that may be related thereto.

FOREWORD

This final report on the Fiber Optic Sensor System was prepared by Rockwell International Science Center under contract F04611-86-C-0036 with the Air Force Astronautics Laboratory (AFAL), Edwards Air Force Base CA. The AFAL Project Manager was Capt John Ward.

This report has been reviewed and is approved for release and distribution in accordance with the distribution statement on the cover and on the DD Form 1473.

JOHN M. WARD, Capt, USAF
Project Manager

L. KEVIN SLIMAK
Chief, Subsystems Branch

FOR THE DIRECTOR

ROBERT L. GEISLER
Director, Aerospace Vehicle Systems Division

REPORT DOCUMENTATION PAGE

Form Approved
OMB No. 0704-0188

1a. REPORT SECURITY CLASSIFICATION UNCLASSIFIED	1b. RESTRICTIVE MARKINGS
2a. SECURITY CLASSIFICATION AUTHORITY	3. DISTRIBUTION/AVAILABILITY OF REPORT Approved for public release; distribution is unlimited.
2b. DECLASSIFICATION/DOWNGRADING SCHEDULE	
4. PERFORMING ORGANIZATION REPORT NUMBER(S) SC5463.FRD	5. MONITORING ORGANIZATION REPORT NUMBER(S) AFAL-TR-88-102
6a. NAME OF PERFORMING ORGANIZATION Rockwell International Science Center 6b. OFFICE SYMBOL (If applicable)	7a. NAME OF MONITORING ORGANIZATION Air Force Astronautics Laboratory
6c. ADDRESS (City, State, and ZIP Code) 1049 Camino Dos Rios Thousand Oaks, CA 91360	7b. ADDRESS (City, State, and ZIP Code) VSSS Edwards AFB CA 93523-5000
8a. NAME OF FUNDING/SPONSORING ORGANIZATION 8b. OFFICE SYMBOL (If applicable)	9. PROCUREMENT INSTRUMENT IDENTIFICATION NUMBER F04611-86-C-0036
8c. ADDRESS (City, State, and ZIP Code)	10. SOURCE OF FUNDING NUMBERS PROGRAM ELEMENT NO. 62302F; PROJECT NO. 2864; TASK NO 00; WORK UNIT ACCESSION NO. EC
11. TITLE (Include Security Classification) Fiber Optic Sensor System (U)	
12. PERSONAL AUTHOR(S) Schoenwald, J. S.	
13a. TYPE OF REPORT Final	13b. TIME COVERED FROM 86/5/30 TO 88/6/1
14. DATE OF REPORT (Year, Month, Day) 89/03	15. PAGE COUNT 38
16. SUPPLEMENTARY NOTATION	

17. COSATI CODES		
FIELD	GROUP	SUB-GROUP
22	02	7

18. SUBJECT TERMS (Continue on reverse if necessary and identify by block number)
Fiber Optic Sensors, Smart Structures, Flexible Structures, Optical Time Domain Reflectometry (OTDR), Microbend Sensors

19. ABSTRACT (Continue on reverse if necessary and identify by block number)

We describe the design, development, and performance of a microbend fiber optical domain reflectometry (OTDR) based distributed strain sensor. A test bed has been developed to evaluate and compare this system to conventional discrete strain gauge sensors. The test bed consists of an aluminum cantilever beam to which have been attached several pairs of strain gauges (for reference) and several microbend transducers. A single standard multi-mode optical fiber is threaded through the microbend transducers. The fiber is pulse illuminated by a commercial OTDR instrument. The microbend losses are detected as step changes in the return OTDR signal waveform. The transducers consist of small pairs of opposing sets of teeth, one set mounted on the flexible beam test bed, the other machined into a small, rigid cantilever bar mounted to produce scissor action as the beam flexes. The transducers are biased to produce a step loss with the beam in its neutral position. The direction of beam deformation is then determined by the increase or decrease of the step size. Several transducers along the beam, incorporating the same fiber, permit the...

20. DISTRIBUTION/AVAILABILITY OF ABSTRACT ☒ UNCLASSIFIED/UNLIMITED ☐ SAME AS RPT. ☐ DTIC USERS	21. ABSTRACT SECURITY CLASSIFICATION UNCLASSIFIED
22a. NAME OF RESPONSIBLE INDIVIDUAL John M. Ward, 1LT, USAF	22b. TELEPHONE (Include Area Code) (805) 275-5205 22c. OFFICE SYMBOL VSSS

Block 19 (continued): acquisition of strain measurements from multiple locations on the structure by processing a single OTDR waveform. The waveform is obtained as the logarithm of the Rayleigh backscattering intensity. The change in the step response of the logarithmic signal caused by each transducer is linear in the in-plane strain produced by displacing the tip of the beam. Repeatability, hysteresis, and sensitivity are dependent on the nature and thickness of the fiber coating, signal processing, transducer design, and other less significant factors. We have demonstrated a resolution of ± 1 microstrain over a range of ± 25 microstrains using transducers with 2 mm pitch in tooth spacing and a 2.5 cm interaction lengthm mounted on cantilever bars 5 cm in length, and averaging multiple waveforms to improve signal-to-noise ratio.

Table of Contents

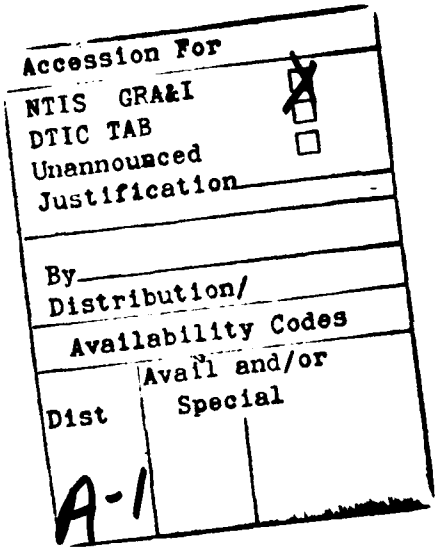

List of Figures

INTRODUCTION

Current approaches to sensing for control of large flexible structures typically involve the use of discrete sensors, e.g., accelerometers and strain gages, or remote sensing such as laser scanning. These techniques, which have been successful for laboratory characterization, will prove to be limiting for very large structures in orbit. Discrete point sensing has the drawback of requiring many sensor elements to adequately monitor all modes of vibration that a structure may encounter. An accelerometer residing at a standing node of one vibrational mode will not detect any signal pertinent to that mode of vibration. A further drawback is that point-to-point hardwiring of many sensor elements is required which could adversely affect the following:

1) Total system weight ;
2) Cost of installation;
3) Structural intrusiveness; and
4) Reliability.

In addition, significant digitizing and computing resources must be dedicated to perform data acquisition from each sensor and construct a map of the state of the structure.

An ideal monitor of structural deformation would have the following characteristics:

1) A single, continuous distributed sensing element;
2) Capable of measuring magnitude and location of strain or absolute deflection;
3) Structurally non-invasive and contribute negligible mass; and
4) Possess signal processing capabilities to identify all pertinent modes of vibration, their magnitudes and frequencies from dc through some maximum, beyond which the excitation response function can be neglected.

SCOPE OF WORK

The scope of work was proposed to establish a test facility to study the feasibility of strain/deformation mapping of large structures using a single continuous fiber optical sensor. The principal tasks include:

Task 1

a) Develop the code for a model of strain for a cantilevered beam under simple transverse deflection, i.e., compute strain for arbitrary deflection and provide graphical output.

b) Provide variable scaling factors to predict the deflection of the beam at any linear position for arbitrary beam length or thickness, given the strain map.

c) Develop inverse code for predicting spatial map of internal strain versus instantaneous beam deformation condition.

d) Design complete experiment: include structural configuration of cantilever beam facility, conventional sensor data acquisition and analysis system and fiber optic sensor system.

Task 2

a) Install a cantilever beam testbed equipped with standard accelerometers and/or strain gages, data acquisition and signal processing hardware.

b) Develop signal processing software to measure and analyze static and dynamic beam state; provide graphical representation of data.

Task 3

a) Apply continuous optical fiber sensor to a cantilevered beam and construct a spatial correlation map between the linear coordinate along the fiber and the planar map of the beam.

b) Investigate requirements for obtaining satisfactory gage response in the optical time domain reflectometry signal due to microbending effects in the fiber.

c) Extend software of subtask 2a) to read and analyze OTDR signal; generate a spatial deformation map from the optical data and correlate with discrete sensors, as appropriate, and with model developed in Task 1.

d) Provide an experimental estimate of the minimum strain/ deflection the sensor can measure and its dynamic range. Assess the computational needs to process the data in real time for various bending frequencies.

TEST AND DEVELOPMENT FACILITY

The following is a list of equipment which was integrated to form a test facility for development of a fiber optic distributed strain sensor:

1) Laser Precision Optical Time Domain Reflectometer;

2) Tektronics 468 Digital Data Acquisition Oscilloscope (IEEE-488);

3) Data Precision 6000 Digital Data Acquisition and Signal Processing System (M68000 CPU based);

4) HP 9816 (M68000) microcomputer for data acquisition and signal processing;

5) HP Multiprogrammer with 33 KHz and 200 KHz high speed A/D converters and channel scanners; and

6) IBM PC-AT compatible desktop computer with data acquisition analog to digital (A/D) card.

DISCUSSION

This program investigates the use of a single multimode optical fiber as a distributed sensor for the purpose of detecting dc and low frequency vibrational deflection of large beams that may constitute the load bearing elements of large space structures. A light weight, effectively non-invasive system with a minimal number of components to maximize reliability, appears feasible with this approach.

Single mode fibers have found applications in sensitive detection of pressure waves, acoustic emission, and inertial rotation, but these all rely on a phase measurement made relative to a reference fiber, and the measured effect is integrated over the length of the sensing fiber, and thus does not lend itself well to the spatial mapping of strain fields.

The method developed here relies on the application of optical time domain reflectometry in a multimode optical fiber to observe the magnitude and location of a structural distortion. The mechanism consists of inducing a microbend (or change thereof) in the optical fiber where the local strain occurs. The optical fiber can be distributed along and around the structure to detect various components of flexure, including torsion and longitudinal extension.

The spatial location of strain is contained in the time domain return signal. A short pulse of incident light is Rayleigh backscattered from the entire length of the fiber to a photosensitive diode. The return signal intensity is proportional to the forward incident power. Microbending in the fiber attenuates this forward power, with resultant attenuation of the return signal. When properly configured, modeled and calibrated, a fiber optic sensor is capable of providing the position and magnitude of strain or distortion throughout the structure to which it adheres.

We now develop a model of strain displacement relationships, and derive the actual quantities measurable by the sensor system.

We will briefly examine the stress-strain relationships of a cantilevered beam to give context to the implementation of the sensor concept. Figure 1 indicates the relevant geometrical features of a cantilever beam. The optical fiber is mounted on either side of the beam at the surface. When a beam is subjected to bending, the surface of one side elongates, while the surface on the other side is placed in compression. These changes in length are a consequence of both the deflection and the finite thickness of the beam.

The elastic curve is the curve taken by the neutral axis. The radius of curvature r taken by the neutral axis at any point is given by

$$r = E I / M, \tag{1}$$

where M is the bending moment, I is the moment of inertia of the beam, E is the modulus of elasticity, or Young's modulus,

$$E = \text{unit stress/unit deformation} = Pl / Ae, \tag{2}$$

where e/l is the longitudinal deformation e per longitudinal distance l. P/A is the stress, or force per unit area applied longitudinally.

A beam bent to a circular curve of constant radius has a constant bending moment. Replacing r in Equation (1) by its approximate geometrical value, $1/r = d^2y/dx^2$, the (approximate) fundamental equation from which the elastic curve of a bent beam can be devel-

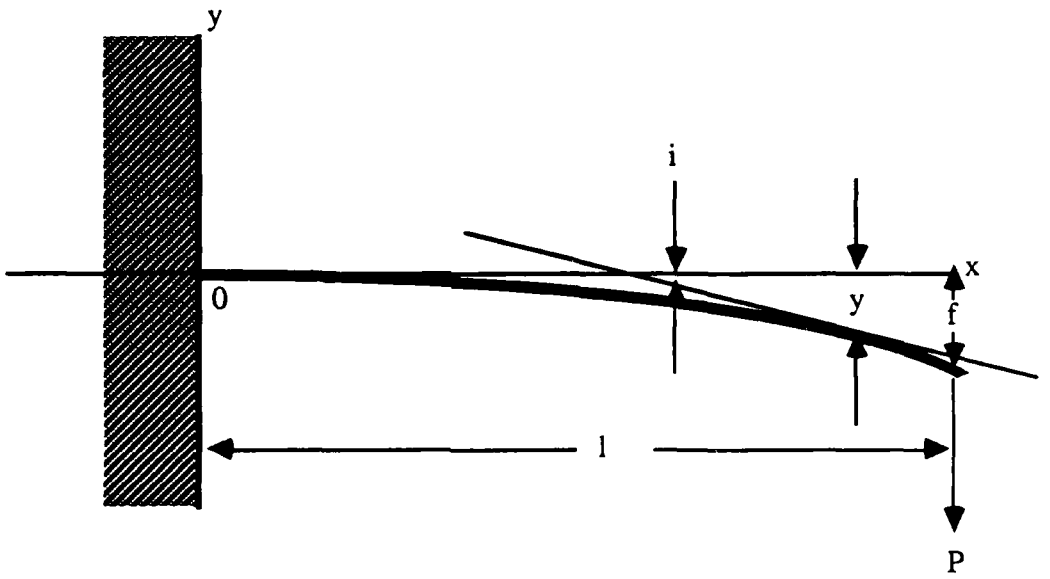

Figure 1 Cantilevered beam

oped and the fundamental deflection of any beam obtained is:

$$M = EI\ d^2y/dx^2 \quad (3)$$

Substituting the value of M in terms of x, and integrating once, gives the slope of the tangent to the elastic curve of the beam at point x;

$$\tan i = dy/dx = \int_0^x M\,dx/EI \quad (4)$$

Since i is usually small, tan i = i, expressed in radians. A second integration gives the vertical (as drawn) deflection of any point of the elastic curve from its original position.

A concentrated load P at a distance l from a clamped origin causes a deflection f at the end of the beam. The bending moment M is

$$M = EI\ d^2y/dx^2 = -P(l - x). \quad (5)$$

Integrating, as described above, and requiring the boundary conditions that dy/dx = 0 when x = 0, yields

$$EI\ dy/dx = -Plx + Px^2/2 . \quad (6)$$

A second integration, with y = 0 when x = 0, yields the elastic deflection

$$EIy = -Plx^2/2 + Px^3/6 . \quad (7)$$

Equation (7) is the elastic deflection curve for the beam neutral axis. As stated at the beginning of this elementary analysis, one side of the beam elongates, placing the local volume in tension, while the other side is in compression. If y can be determined as a function of x, then, for a beam of known length l and material property E, the driving force P can be deduced, and a reaction force applied to extinguish the deflection.

A sensor capable of measuring the strain at the surface, together with a model of the location of the beam neutral axis, would enable the calculation of the deflection of the beam neutral axis. This in turn would provide the information necessary to reconstruct the deflection state of the beam.

The beam is now generalized to account for its finite thickness, which results in (internal) inplane (i.e., in the plane of the beam) strains. We will show how the various strains are a function of distance from the neutral axis. For a symmetrical beam, having uniform cross-sectional material and elastic properties, and simple rectangular geometry, the neutral axis coincides with the midplane of the beam.

We now review the results of a derivation of strain displacement relationships described elsewhere[1] for simple cantilever bending about one axis.

The equations which relate the strain at any point in a beam undergoing some deformation will be developed in this section in terms of the displacements at the geometrical midplane of the beam (u_o, w_o) and the displacement in the y-direction (v). We follow the notation convention that the ordered set (u, v, w) are displacements along the (x, y, z) axes.

Consider a section of the beam in the x-y plane, Figure 2, which is deformed due to some loading in the y-direction. We assume the point A at the geometrical midplane undergoes some displacement u_o in the x direction. Furthermore, we assume that the line BAD, the normal (perpendicular) to the geometrical midplane, remains straight and normal to the deformed midplane. This is equivalent to neglecting shearing deformations, which is a practical assumption considering the deflection modes of the beam that are likely to occur under normally incident perturbations or impacts. With this assumption, the displacement of any point on the normal BAD (say of line C) is given by the linear relationship

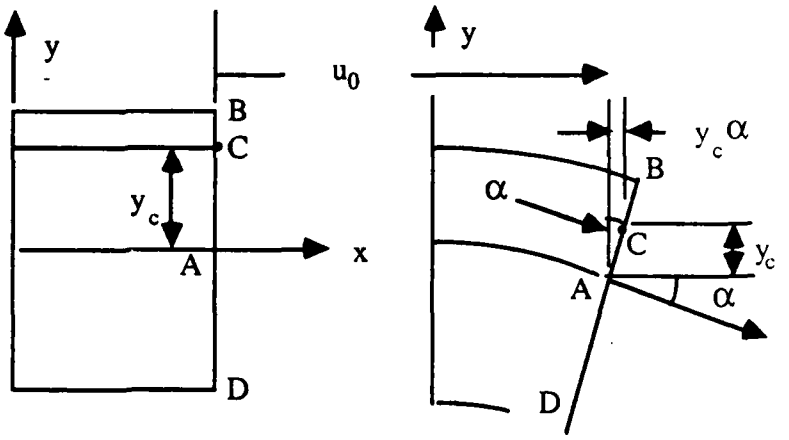

Figure 2 Cross-section of a segment of a cantilever beam before and after bending in the x-y plane

$$u_c = u_o + y_c\alpha, \tag{8}$$

where, as shown in Figure 2, y_C is the y coordinate of the point C measured from the geometrical midplane, and α is the slope of the normal BAD with respect to the original vertical line. By similar triangles, α is also shown to be the slope of the midplane with respect to the y-axis, or

$$\alpha = \partial v/\partial x, \tag{9}$$

where the slope is the rate of change of the deflection in the y direction with respect to change in the x direction. Combining Equations (8) and (9), we obtain an expression for the displacement u in the x direction for an arbitrary point at a distance y from the midplane:

$$u = u_o + y\, \partial v/\partial x, \tag{10}$$

where the slope is the rate of change of the deflection in the y-direction with respect to change in the x direction.

In a completely analogous manner, the displacement w in the z-direction of an arbitrary point at a distance y from the geometrical midplane is

$$w = w_o + y\, \partial v/\partial z, \tag{11}$$

where now w_o is the midplane displacement in the z direction. Equations (10) and (11) give the inplane displacements (x,z directions) of any point in the beam in terms of the inplane displacements at the geometrical midplane (u_o, w_o) and the deflection v in the y-direction.

We have made the simplifying assumption that the beam thickness BAD remains constant in length and undeformed, apart from an alteration in direction. Thus, the value of the normal strain, ε_y, may be neglected when considering normal deflections and v represents the normal deflection of the beam without regard to the y coordinate within the beam along the normal BAD. Similar arguments can be made to show that we may also neglect the shear strains γ_{xy} and γ_{yz}. Again, this is reasonable due to the assumption that, for the moment, we are only considering beam flexure in one direction.

The beam will experience tension on its upper surface and compression on its lower surface. The normal strain in the x direction is defined as the change in length divided by the original length. Recalling that the change in length of a line segment is equal to the relative displacement of the two ends, the normal strain is

$$\varepsilon_x = \lim_{\Delta x \to 0} \Delta u/\Delta x = \partial u/\partial x. \tag{12}$$

Using Equations (10) and (12) together, we may obtain a relationship between the normal strain $\varepsilon_x(y)$ at any distance y from the midplane and the strain at the midplane:

$$\varepsilon_x(y) = \partial u/\partial x = \partial u_o/\partial x + y\, \partial^2 v/\partial x^2. \tag{13}$$

We point out that the term $\partial^2 v/\partial x^2$ is the beam curvature and is equal to $1/r$, where r is the radius of curvature.

$\partial^2 v/\partial x^2$ and $\partial v/\partial x$ are the curvature and slope of the midplane axis, respective-

ly. The midplane axis is identical to the neutral beam axis for simple symmetrical geometries. Equation (13) may now be rewritten as

$$\varepsilon_x \pm(y_s,x) = \partial u/\partial x^{\pm} = \partial u_o/\partial x \pm y_s\, \partial^2 v/\partial x^2, \tag{14}$$

where the $\pm$ corresponds to the top or bottom surface of the beam, at $y = \pm y_s$. If we take the difference of the strains measured on opposite sides of the beam at the same value of x, we obtain

$$\varepsilon_x+(y_s,x) - \varepsilon_x-(-y_s,x) = 2y_s\, \partial^2 v/\partial x^2. \tag{15}$$

We shall call the difference of terms on the left side of Equation (15) $[\Delta\varepsilon(x)]$. Equation (15) may then be rewritten

$$[\Delta\varepsilon(x)] = 2y_s\, \partial^2 v/\partial x^2, \tag{16}$$

where $[\Delta\varepsilon(x)]$ is a measured quantity and $2y_s$ is simply the thickness of the beam. Of interest now is the value of v as a function of x. By integrating twice we may find the net deflection of the beam midplane at any position x, since v is the deflection of the beam in the y-direction. The first integration yields

$$\int_0^x [\Delta\varepsilon(x)]\, dx = 2y_s \{\partial v(x)/\partial x - \partial v(x=0)/\partial x\}. \tag{17}$$

For a beam clamped at the origin (x=0) we may observe by inspection that $\partial v(x=0)/\partial x$ equals zero, so that the last term disappears. A second integration, with $v = 0$ when $x = 0$, results in

$$\int_0^{x'}\int_0^x [\Delta\varepsilon(x)]\, dx\, dx' = 2y_s\, v(x)\,. \tag{18}$$

The quantity v(x) is recognized as simply the net y-deflection of the beam referred to earlier. Equation (11) is a compact relationship between the deflection v at x and the doubly integrated differences of paired strain measurements made along the beam over the range from zero to x. If $[\Delta\varepsilon(x)]$ can be measured as a continuous function of x, then the accuracy with which v(x) can be computed is limited only by the fineness with which x is divided for numerical integration purposes. As a practical matter, the analog signal $[\Delta\varepsilon(x)]$ will be processed by A/D conversion, followed by digital signal processing. This now leads into a discussion of how $[\Delta\varepsilon(x)]$ is acquired using a single optical fiber.

IMPLEMENTATION OF A FIBER OPTIC STRAIN MAP SENSOR

The technique of optical time domain reflectometry is a standard commercial method of testing the continuity of optical fiber communications lines. A short and intense pulse of laser light is injected into one end of the fiber (multimode, in this case). The forward traveling pulse is continuously backscattered toward the source due to Rayleigh Scattering. The origin of Rayleigh Scattering is due to residual impurity scattering sites on the scale of atomic size. The intensity of backscattering is proportional to the forward power, pulse width and scattering cross-section of the medium.

When an optical fiber is illuminated by a source, usually a diode laser or LED, light is captured by the core and wave guided subject to the conditions of total internal reflection at the interface between the core region and cladding. These conditions are mathematically identical to those which prevail in microwave guides. The light will initially be in some state determined by the nature of illumination, but the normal bending and imperfections in a standard high quality fiber will soon cause the energy to populate an equilibrium distribution of possible modes. Further bending and internal scattering will result in a continuous mixing and weaving of energy between the numerous modal states.

When the fiber is perturbed from its cylindrical symmetry at some point along the fiber, this modal redistribution occurs. Some of the light will couple to radiative modes and escaped from the fiber. Thus, the forward power is reduced, and the Rayleigh backscattering, which is proportional, is observed to decrease at that point.

Observation of the Rayleigh backscattered energy is made by placing a beam splitter between the fiber and the source and and directing the returned energy at a high speed detector. In this way, the return signal is time expanded in proportion to the length of the optical fiber, and the detector signal can be displayed on an oscilloscope as a function of time. The return signal will display any evidence of fiber distortion or damage by a drop in the return signal at the point corresponding to the time it takes for light to travel through the fiber to that defect.

A practical solution is the high speed digitization of the waveform. The digitized waveform can be processed to extract the strain map and physical state of the structure.

The fiber, when properly applied to a structure, can be bonded in a manner that will cause deformation of the fiber when the structure undergoes flexure. The method of application actually involves the use of a small transducer, a drawing of which is shown in Figure 3. A photograph of the actual transducer used is shown in Figure 4. It consists of two components through which the fiber passes. Each component has a jaw with a set of serrations, and the two serrated surfaces are complementary so as to deform the fiber in a periodic fashion when compressed between the two elements. One part is attached to the structural surface under consideration in the region over which the fiber passes. The other portion is cantilever mounted to the beam at a distance (typically 2.5 - 5 cm) from the first component such that a clamping action is generated by the jaws. The upper (cantilevered) component provides a relatively rigid element against which the fiber is pressed with greater or lesser force as the beam deflects. The transducer is biased to give a net signal when there is no net deflection in order to distinguish between compressive and tensile inplane strain. The use of a repeated grooved structure enhances the sensitivity of the transducer element.

The transducer itself can be quite small, on the order of 12.5 cm x 5 cm and 0.1 - .5 cm thick. Application could be with adhesives, threaded screws, rivets, etc. Adhesives offer the least invasive and perturbing method of application.

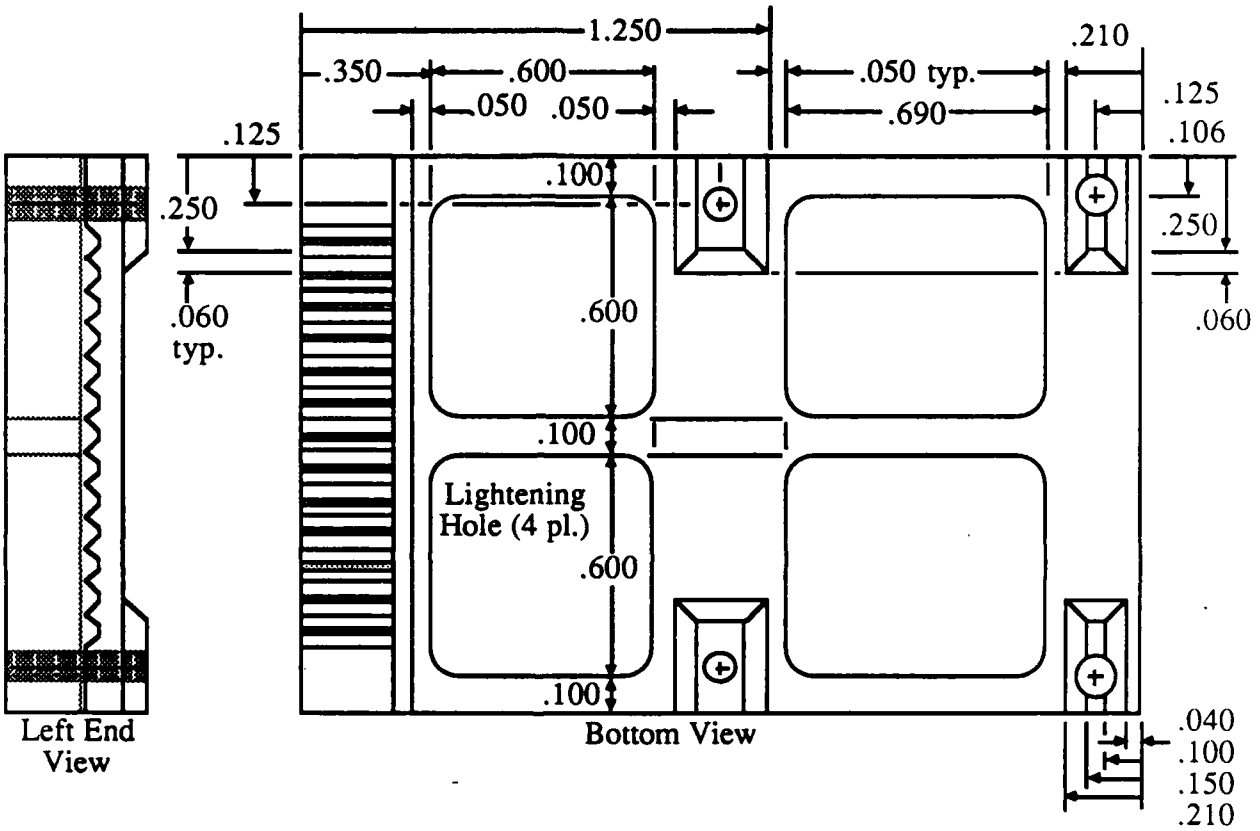

Figure 3 Design of transducer which is mounted at several sites on cantilever beam

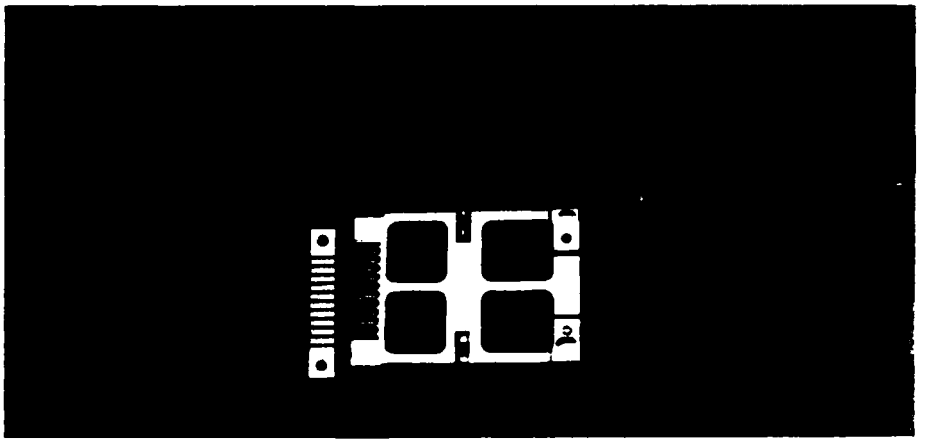

Figure 4 Photograph of transducer

DESCRIPTION OF THE SYSTEM CONFIGURATION

Seven pairs of strain gages were attached to the cantilevered beam and, after signal conditioning, their output fed to a 16 channel A/D card in the HP multiprogrammer, capable of reading 16 individual analog input voltages at a rate of 32 kHz or 8 differential pairs of voltages at 16 kHz. The OTDR signal was read and digitized by either a TEK 468 or a DP6000. Since the vibrational modes of the beam were designed to remain generally under 20 Hz, there is no significant sampling problem. Alternatively, the multiprogrammer/ scanner system can perform the same function.

The discrete sensors monitor the motion concurrently with the fiber optic system. They provide concurrent verification of the model encoded to predict beam disposition based on fiber optic sensor data acquired. Figure 5 is a functional representation of the facility, showing the relationship between the beam, discrete and fiber optical sensors, data acquisition and signal processing systems.

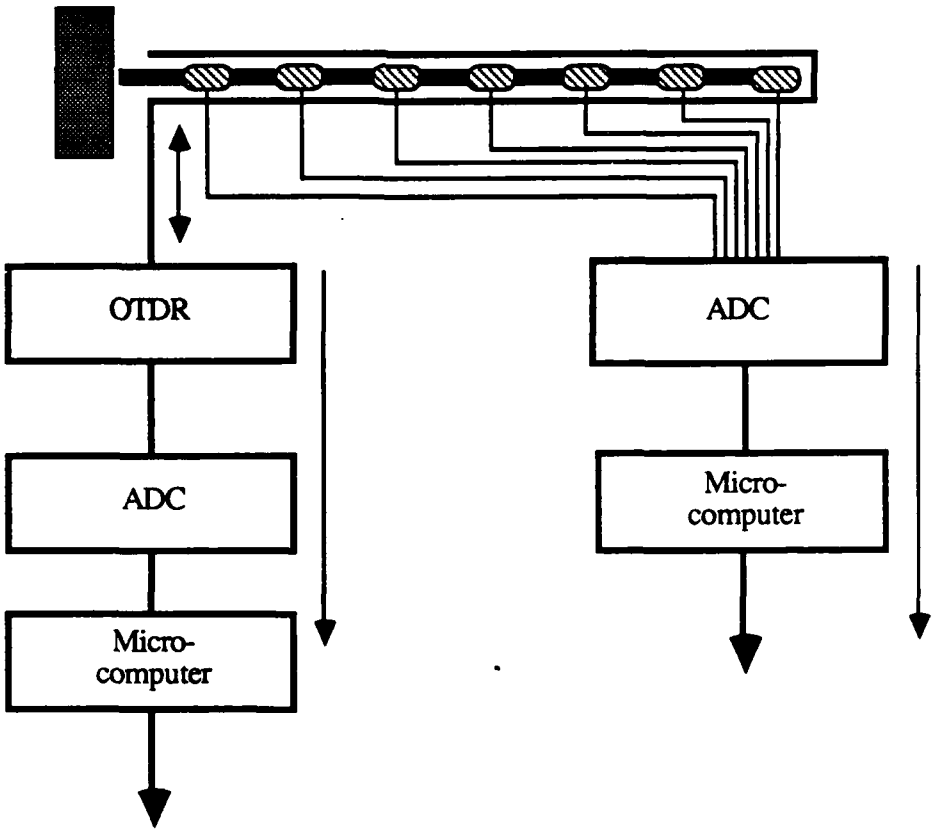

Figure 5 Diagram of flexible beam testbed for fiber optic sensor development

TESTBED STRUCTURE

A testbed structure (Figures 6 and 7) was fabricated to investigate the performance of the fiber optic sensor system. The beam itself was made of 6061-T6 aluminum bolted between two low carbon steel channel beams for support, which were then mounted on a base of low carbon steel. The mass and rigidity of the channel beams and base plate are high enough that the cantilever modes of the beam are the only ones of significance. Beam dimensions are such that torsional modes can also be neglected.

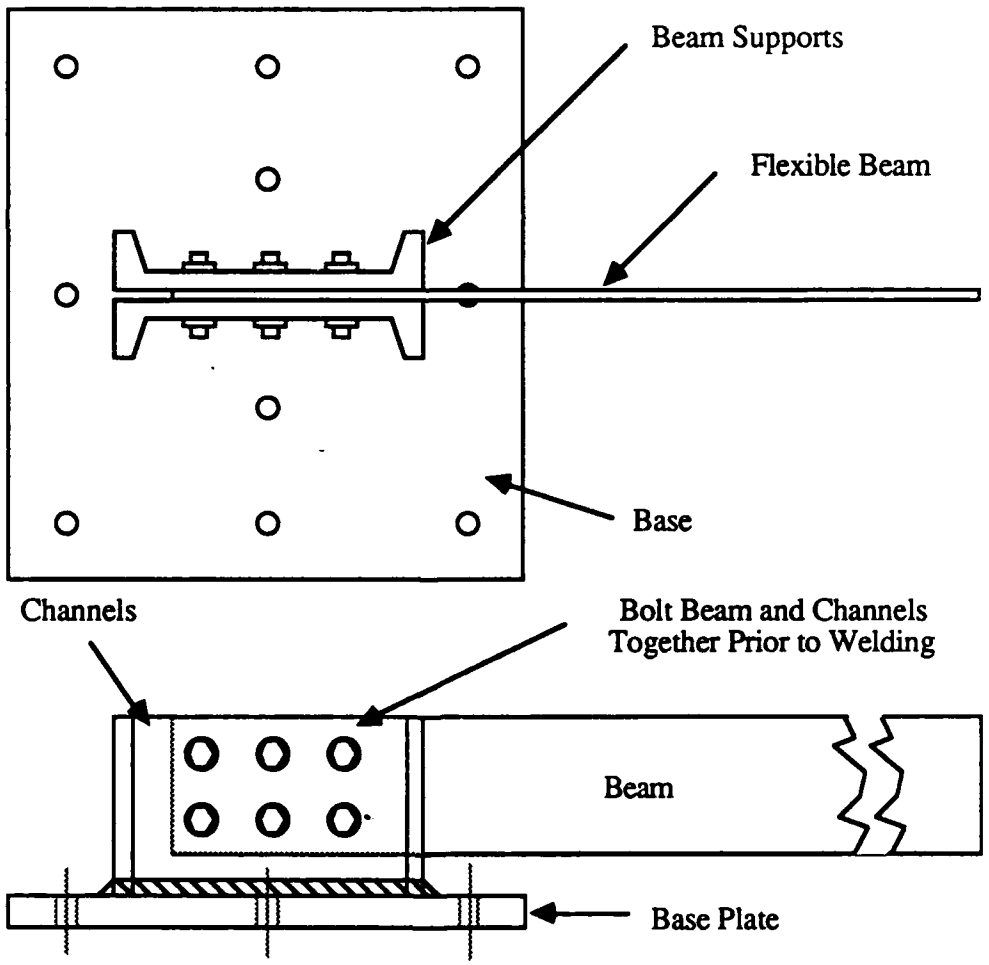

Figure 6 Illustration of fabricated cantilever testbed

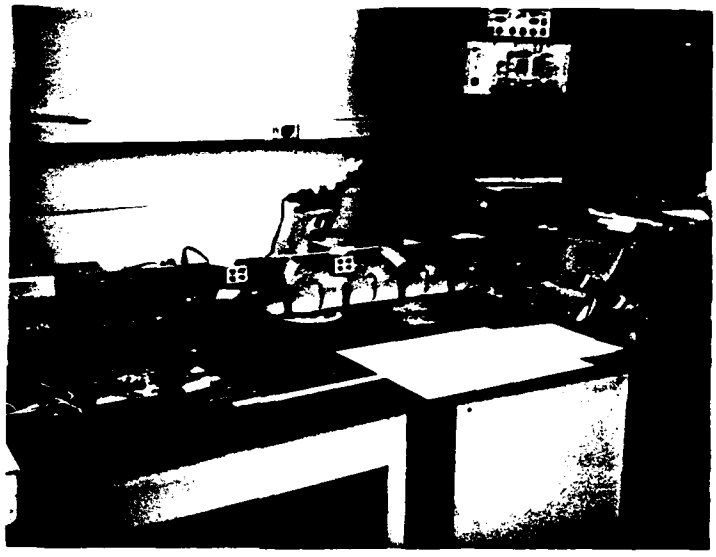

Figure 7 Distributed strain sensor testbed

The testbed includes an array of conventional resistive strain gages that served as a reference to the fiber optical system. Figure 8 is a diagram of the data signal acquisition system that was used to acquire conventional strain gauge data. The multiplexer and A/D converter shown in the diagram are actually an integrated multichannel data acquisition card installed in the microcomputer system. The balanced bridges and amplifiers are a custom design. A detailed schematic of the 8 channel strain gage bridge amplifier is shown in Figure 9. The BNC cable output for each channel is input to a channel of the analog-to-digital (A/D) card in the microcomputer. Seven (of a maximum of eight possible) pairs of strain gages were attached to the beam at equal intervals along its length. A polynomial fit to a model of simple lateral tip deflection of the beam was used to obtain parameters to generate deflection, slope and curvature information from the strain gage data.

A flow diagram for the computer controlled acquisition of OTDR and strain gage array data is shown in Figure 10.

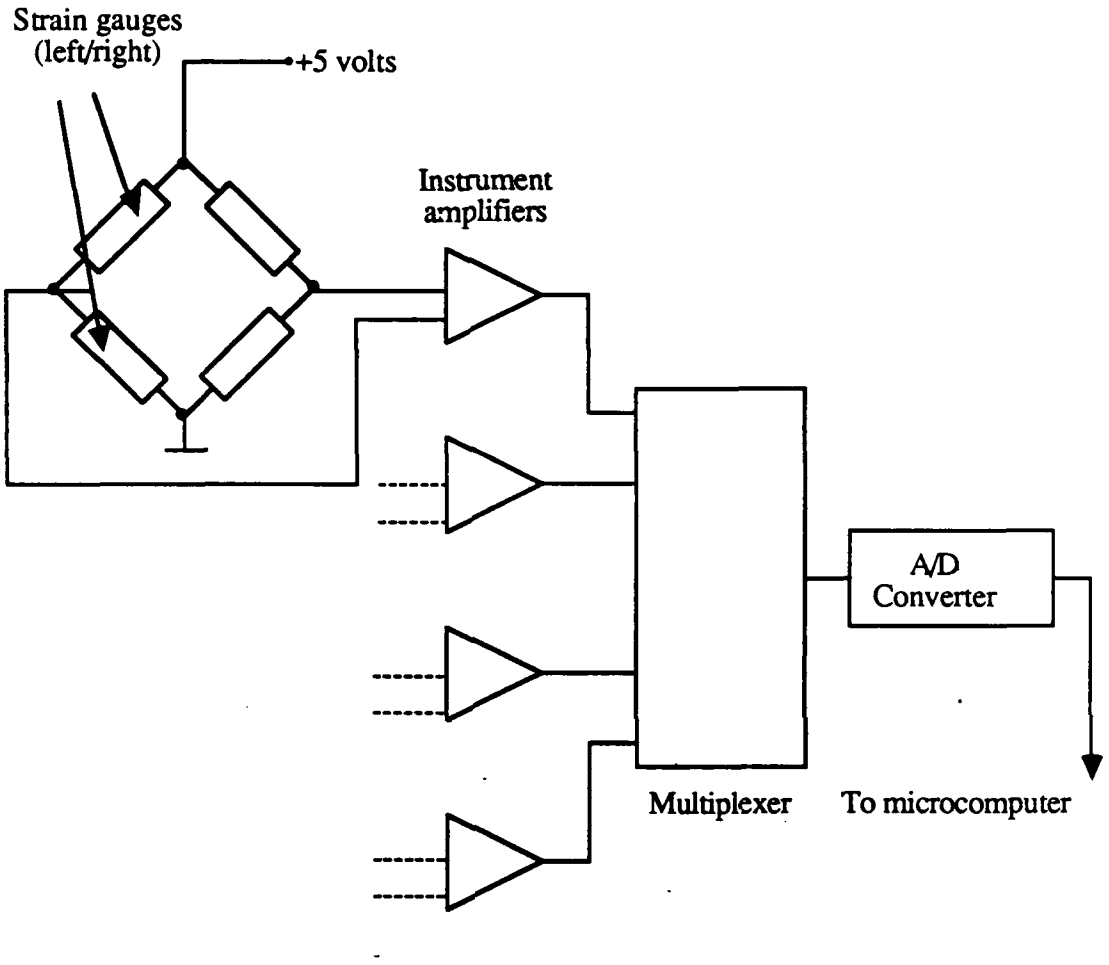

Figure 8 Strain gage signal data acquisition system

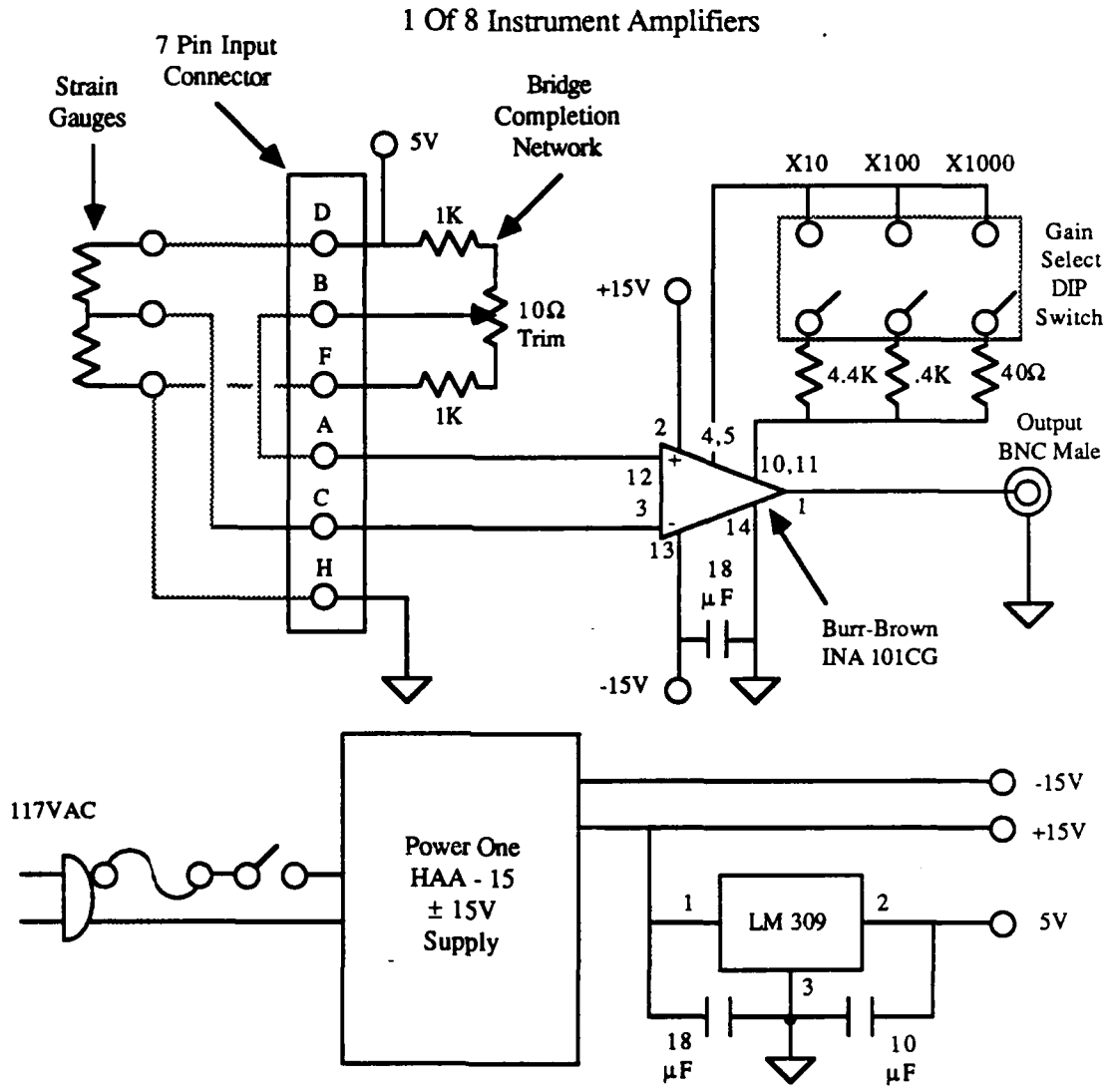

Figure 9 Detailed schematic of the 8 channel strain gage bridge amplifier

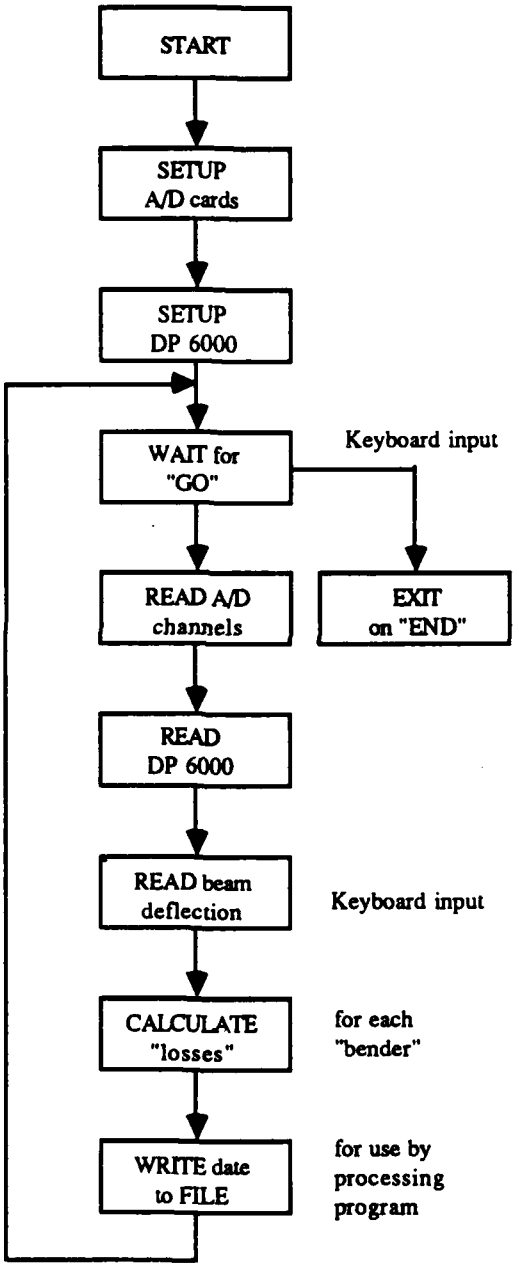

Figure 10 Flow diagram for the computer controlled acquisition of OTDR and strain gage data. "Bender" refers to microbend transducer

OPTICAL FIBER MICROBENDING SENSITIVITY

Measurements performed by Asawa, et al,[2] enable an estimate of the sensitivity expected with the system configuration described in this document. Asawa observed a 2 dB change in signal for a local deformation corresponding to a radius of curvature of 1 km. Assuming a simple circular deflection shape for a beam 1 meter long, this would produce a lateral deflection of 1 mm and subtend an angular deflection of 1 milliradian. The actual deformation of the optical fiber in the microbending transducer was 5 microns.

Sensitivity of the transducer is proportional to the number of corrugations in the microbending transducer and the periodicity of the corrugations. The measurements described by Asawa were pertain to a "non-resonant" periodicity in the corrugation spacing. The "resonance" period of an optical fiber is a function of the diameters and relative indices of the core and cladding region. Inducing microbending with a resonance period will increase the sensitivity, by as much as a factor of 4 -10. Increasing the number of corrugations can produce a similar gain. As reported by Asawa, the sensor was prototypical and not optimized.

Microbend sensing is accomplished by deforming the fiber between a pair of toothed or serrated plates that introduce small bends in the fiber, as shown in Figure 11. A theoretical analysis of the perturbation of the cylindrical symmetry of the core region of the fiber provides the coupling strength for transferring light from one propagating mode in the fiber core to another, or for scattering out of the core, into the cladding, or out of the fiber

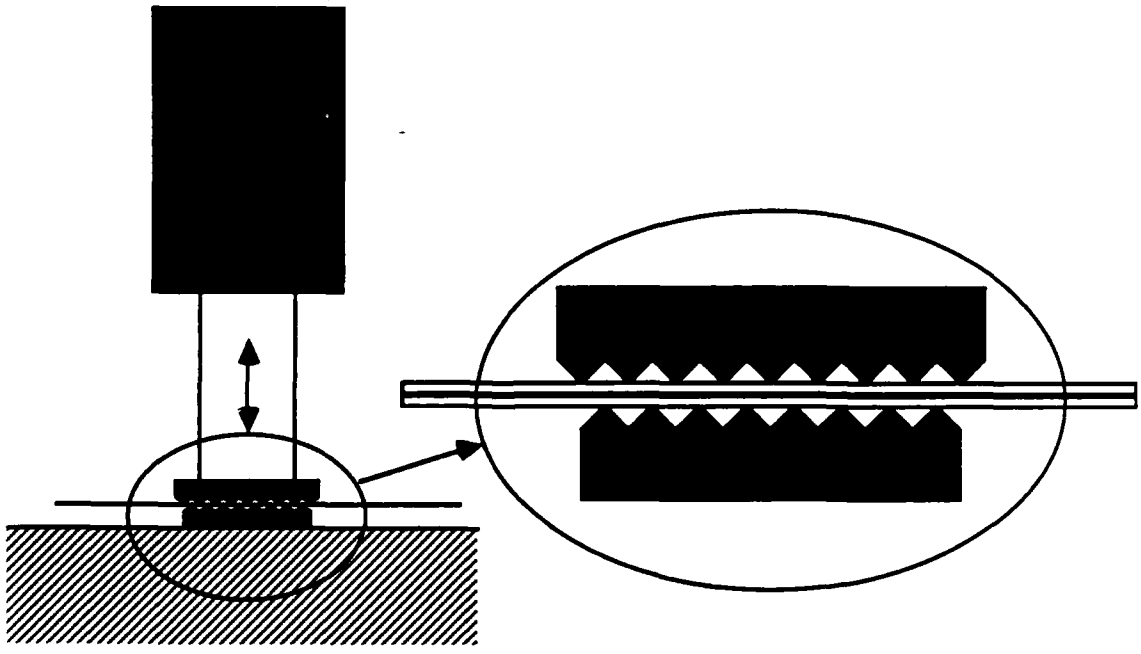

Figure 11 Microbending perturbation of the fiber symmetry is induced by deforming the fiber between two sets of serrated plates

altogether.[3] If the propagation constants of two modes are designated β_1 and β_2, the field dependencies of each behave with time and distance z along the fiber axis as

$$E_1 \sim \exp(i\omega t - \beta_1 z) \text{ and } E_2 \sim \exp(i\omega t - \beta_2 z). \quad (19)$$

The condition for coupling between the two modes is the phase matching between the two propagation constants produced by the serration period L is given by

$$L = \frac{2\pi}{\beta_1 - \beta_2} \quad (20)$$

The efficiency which light scatters between two modes is dependent on the amplitude of the perturbation and the population distribution of propagating modes in the fiber core. This, in turn, depends upon the profile of the optical index of refraction of the core and the index of the cladding surrounding it. The index profiles of multimode fibers are typically step functions or "parabolic." Thus, to excite radiative losses, there can be an optimal period L for a given fiber cross section and index profile.

Three types of microbending designs were investigated. The first one, and the one we returned to for final implementation with minor modification, consisted of two plates with triangular serrations. Three such plate sets were fabricated, with each set having a different pitch to the serration period: 1 mm, 2 mm and 4 mm. The interaction length was 1.25 cm for all transducers. These plates were machined from aluminum. In each set, one plate was rigidly mounted. The other was mounted to a piezoelectric translator having a maximum excursion range of 15 micrometers. The fiber was placed between the two plates and one plate was driven against the other. The step drop introduced in the OTDR signal was measured versus jaw displacement.

The second type of transducer was an attempt to simplify the design and ease of implementation. A commercially available fiber[4] with a polymer filament wrapped in a spiral around the fiber formed an intrinsic microbend sensor. When compressed between two flat surfaces, the fiber sensor was naturally deformed in a manner identical to that which would occur if the fiber were placed between the serrated plates, described above, having the same effect. A difference in performance was noted in that the fibers incorporated in this sensor by the manufacturer had considerably more transmission loss in the unperturbed state and therefore limited its use because of dynamic range considerations. Another characteristic noted was the long term drift of the sensor response over repeated compressions. This was attributed to permanent deformation of the polymer filament spiral. This same effect was noted in the first type of transducer design due to the pointed nature of the serration profile.

In view of the high losses encountered with this fiber, a variation of this design was examined: fine copper wire was spiral wrapped around 2.5 cm segments of the optical fiber with more acceptable attenuation rates. The pitch of the winding could be controlled at our discretion. A pitch of 2 mm was chosen to maintain some normalization with the polymer spiral fibers. Response from this transducer was more favorable and comparable to the serrated design, but maintaining reproducibility of the winding from one transducer to another was problematic, and would require implementation of process control beyond the

immediate interest of this project.

In the final design, the points of the serrated transducers first used were lapped to produce a flat mesa profile. This resulted in less permanent deformation of the polymer buffer protecting the fiber. Over time, such deformation would reduce the effective diameter of the fiber/buffer at the points of contact, shifting the onset of response to compression. Smoothing the profile of the serration reduced this effect and the migration of buffer material in the contact region. A further consideration in the design using sharply profiled serrations is the tendency for the serration points to wear through the buffer and break the silica fiber.

The sensitivity of the three serrated transducers was measured in a microbend test fixture shown in Figure 12. One plate was mounted on a static base which could be manually translated by vernier control. The other plate was attached to a piezoelectric translator, capable of 0 - 15 micrometer displacement. The translator was driven, in turn, by a voltage amplifier/driver. An IEEE-488 computer programmable function generator provided the low voltage input. The analog return OTDR waveform was captured in a 100 MHz IEEE-488 programmable digitizing oscilloscope. The deformation signal is observable as a step down in the OTDR waveform that changes magnitude as the degree of microbending changes. Figure 13 is a plot of the change in the magnitude (in volts) of the OTDR signal as the serrated plates are compressed over a range from 0 to 10 microns. The OTDR signal is linear in the logarithm of the power, so the resulting curve illustrates remarkable log-

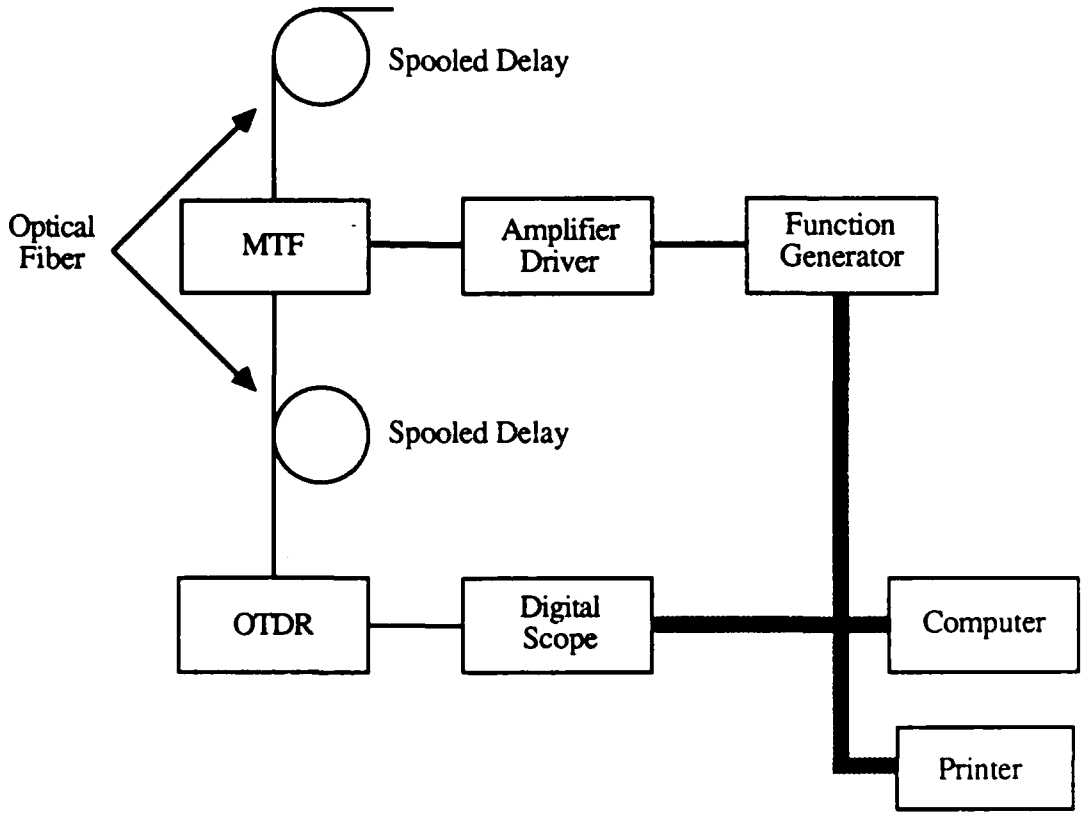

Figure 12 Microbend sensor test system

linearity in response to the microbending effect. Each data point is a 64 sample averaged to improve the signal-to-noise ratio.

These measurements just described take into account the thermal heating of the laser junction, which tends to generate optical power that is very sensitive to temperature. Initial results showed a monotonic shift in the response curves over time toward lower sensitivity. The OTDR now has provisions for thermal stabilization of the laser. When provisions were made for carefully repeating measurements in which the thermal cycling OTDR was moderately repeatable, the data, shown above, was quite well behaved.

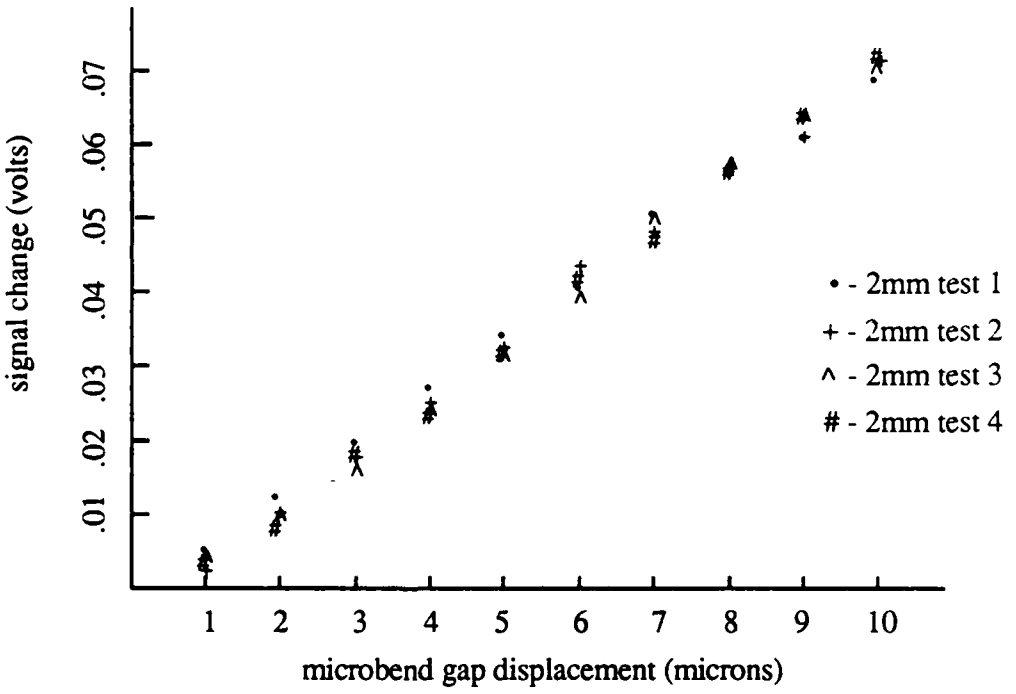

Figure 13 Signal (in volts) of OTDR step change to displacement of microbend

DISTRIBUTED STRAIN TRANSDUCTION

The core problem in proving the concept of OTDR distributed strain sensing is in developing a transducer with which the optical fiber can be mated in a serial array to the structure and impose a measure of the distributed strain effects on the backscattered light signal waveform. A cantilever device was developed, and is shown schematically in Figure 3. It provides for an interaction length of 2.5 cm. A pitch of 2 mm was chosen as a result of best sensitivity observed in the earlier microbend experiments. The cantilever structure had an arm of 5 cm. One serrated surface is firmly affixed to the flexible beam. The other serrated surface is part of the rigid transducer which is mounted as a "diving board." The two sets of serrated jaws meet in a complementary "peak-to-valley" as is required. The fiber ran through the microbend structure. The beam and rigid component form a "scissor," with the fiber squeezed between the two jaws. As the beam flexes, the gap modulates. A shim between the mounting surfaces of the two components and the beam provides for biasing of the microbending when the beam is quiescent. This enables one to distinguish between flexure of the beam in either direction, i.e., the signal step will decrease when the beam is bent in one direction (such that the surface on which the transducer is mounted is placed in tension and the jaws open), and will increase in the other (when in compression, and the jaws close).

The testbed beam could be fitted with as many as four such transducers on each side of the beam, for a total of eight. Our experiments included acquisition of data for up to four transducers, all placed on the same side of the beam. Under simple free vibration, the beam has a strain profile that decreases monotonically with distance from the clamped end. Thus, transducers farther from the fixed end of the beam sense rather low levels of strain. Conversely, higher order modes of vibration can be sensed more effectively by transducers farther from the fixed end as the strain distribution peak shifts away from the fulcrum.

The spatial resolution of the OTDR is limited by the (1) rise/fall time of the laser and detector circuitry, and (2) pulse duration. Increased signal-to-noise ratio is obtained by longer pulses, as the Rayleigh backscattered signal is proportional to the total energy in the forward pulse. The trade-off in sensitivity is in spatial resolution: sharper pulses yield better spatial resolution. The peak signal-to-noise ratio of the OTDR was enhanced by signal averaging. A practical limit exists in that such averaging slows the rate of data acquisition. A choice must be made among these parameters to demonstrate concept feasibility with available instrumentation. The spatial resolution of the OTDR is limited to 5 meters (along the fiber) in the long pulse width mode. The transducers need not be separated by such large distances. In fact, the transducer spacing is eight inches (20 cm) on the beam. A delay line of ~50 ft (~15.25 meters) of optical fiber was coiled between sensor sites. This provided more than enough spatial/temporal separation between transducers to resolve separately the microbending occurring at each site on the beam.

Calibration of the transducers (both resistive strain gages and fiber optic sensor) was performed as follows: the beam was statically deflected at its tip by a fixed, known amount. The various sensor signals provided data for a polynomial coefficient fit to the Equation for the static deflection of a cantilever mounted elastic beam. From then on, digital sampling of the two sensor systems by two independent computers provided the time variant data for dynamic reconstruction of the shape of the beam, its local curvature, strain, strain-rate or velocity-rate, etc.

A typical OTDR signal is shown in Figure 14. At each transducer the fiber is de-

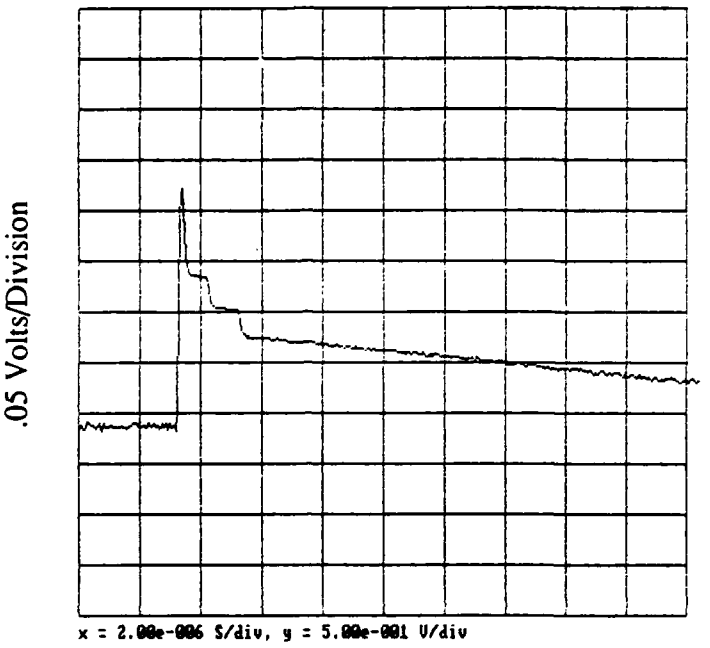

Figure 14 OTDR Waveform showing step signal at two transducers

formed in a biased fashion with the beam strain so that a bipolar signal is obtainable and one can distinguish the direction of strain. Each step corresponds to sensing at another sensor and position along the beam. For a beam in its unstrained state, the measured step in voltage corresponding to each transducer is the set point from which all strain measurements are made. Changes in this voltage indicate the corresponding change in strain, positive or negative. Based upon a simple model for a cantilever beam under simple deflection[1] we can reconstruct the shape of the beam either from the resistive strain gages or the optical fiber sensor. A typical plot for the former is shown in Figure 15.

The results for strain detection in one of the transducers is shown in Figure 16. The plot indicates the change in the voltage drop caused by microbend losses in the fiber as it passes through the serrated section. The "scissor" action induced as the cantilever beam bends causes the jaws to open further or close, depending on the direction of beam deformation. For the transducer used, the dynamic range with linear response is ± 25 microstrains.

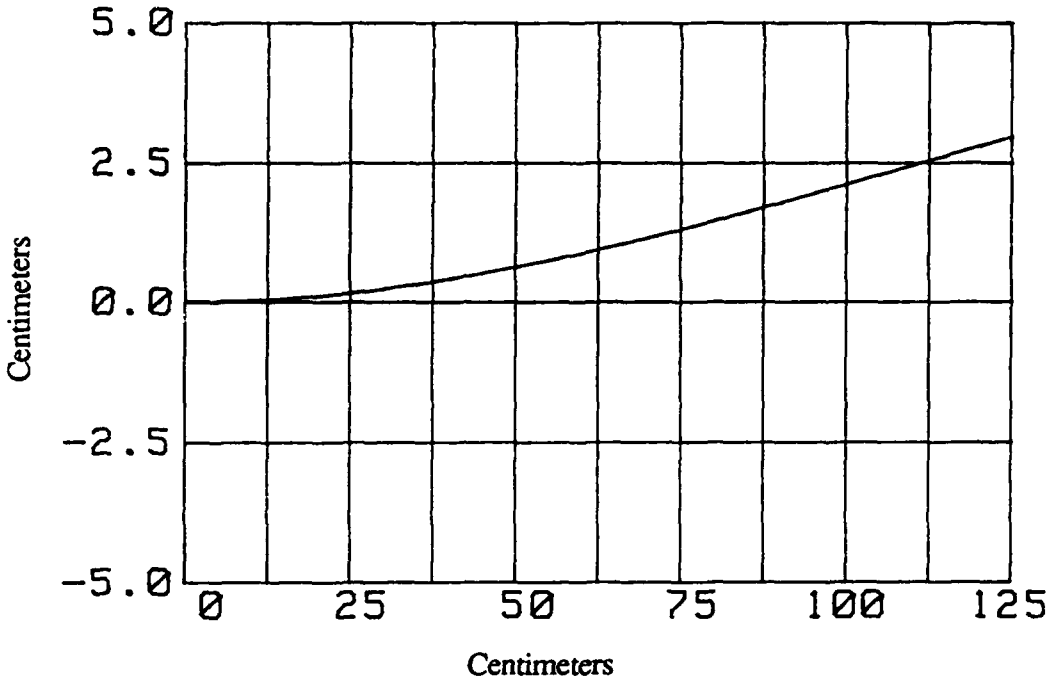

Figure 15 Reconstructed shape of aluminum beam

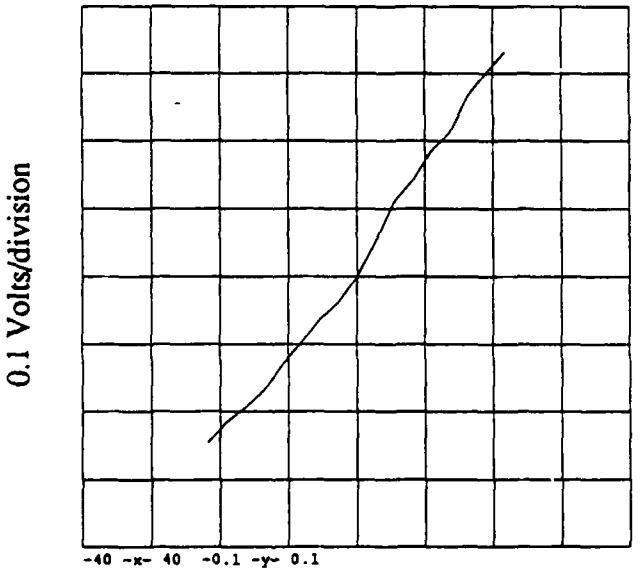

10 μstrains/division

Figure 16 Sensor response versus strain

CUSTOM INSTRUMENTATION

The tradeoffs inherent in the sensitivity and dynamic range of the fiber optic sensor system as regards strain measurement have been discussed above. We briefly list them:

1. Pulse peak power;
2. Pulse duration;
3. Detector noise level and sensitivity; and
4. Fiber attenuation rate.

The total signal to noise budget will then set a limit on the product of the *number of transducers times the dynamic range per transducer*. Digital resolution of the total signal (i.e., number of bits of resolution) will then limit the resolution of each sensor.

Improvements in the dynamic range can be achieved by (1) choosing a laser diode source to increase the pulse peak power, (2) implementing laser junction thermal stabilization, and (3) selection/design of a superior low noise optical receiver.

Spatial resolution is affected by the speed of the laser transmitter and receiver, and time sampling subsystems since rise-time, fall-time and total pulse width of electronics at either end of the fiber limit the time resolution, which is proportional to distance.

Of further interest is the time rate of sampling of the distributed sensor for purposes of determining the frequency spectrum of the vibrating structure. Thus, if a large structure is expected to have significant vibrational properties at frequencies up to 5 Hz, we would like to sample the entire structure at twice the Nyquist frequency, i.e., 20 Hz. The digitizing oscilloscope used was limited to rearming the trigger at a 2 Hz rate. Thus, "real-time" sampling would only be effective for vibrations below 0.5-1 Hz.

Having limited ourselves to the use of a commercial OTDR and digitizing oscilloscope in the current experiments, there was no facility for improving the speed or peak power of the laser, or noise level of the detector, or speed and magnitude of the digital sampling oscilloscope. The one area where customization is easily implemented is in the sampling electronics, shown in Figure 17. While the digital oscilloscope is capable of capturing 1024 points with 100 MHz (100 nanosecond) time resolution and 8 bit amplitude resolution, most of the acquired data is of no value: the measurement of interest is the change in output across the portion of the fiber deformed by the transducer. To measure this change, the output is delayed by a delay line and the undelayed output is subtracted from the delayed output by means of an operational amplifier. An attenuator is placed in the undelayed channel to compensate for the attenuation in the delay line. Low pass filtering is also performed to increase the signal-to-noise ratio.

A sample and hold circuit is used to sample the difference waveform at a point corresponding to the transducer being sampled.

The range counter is started by the start of the laser pulse and counts down a clock. A number proportional to the range of the measurement point is preloaded by the computer. Sampling is started when the range counter reaches zero. Only one transducer is sampled for each laser pulse. A relatively slow A/D converter, such as the one that forms part of the 80197 chip, may now be used to digitize the sample. The 80197 controller is used to further process the samples and generate the desired output as a serial data stream.

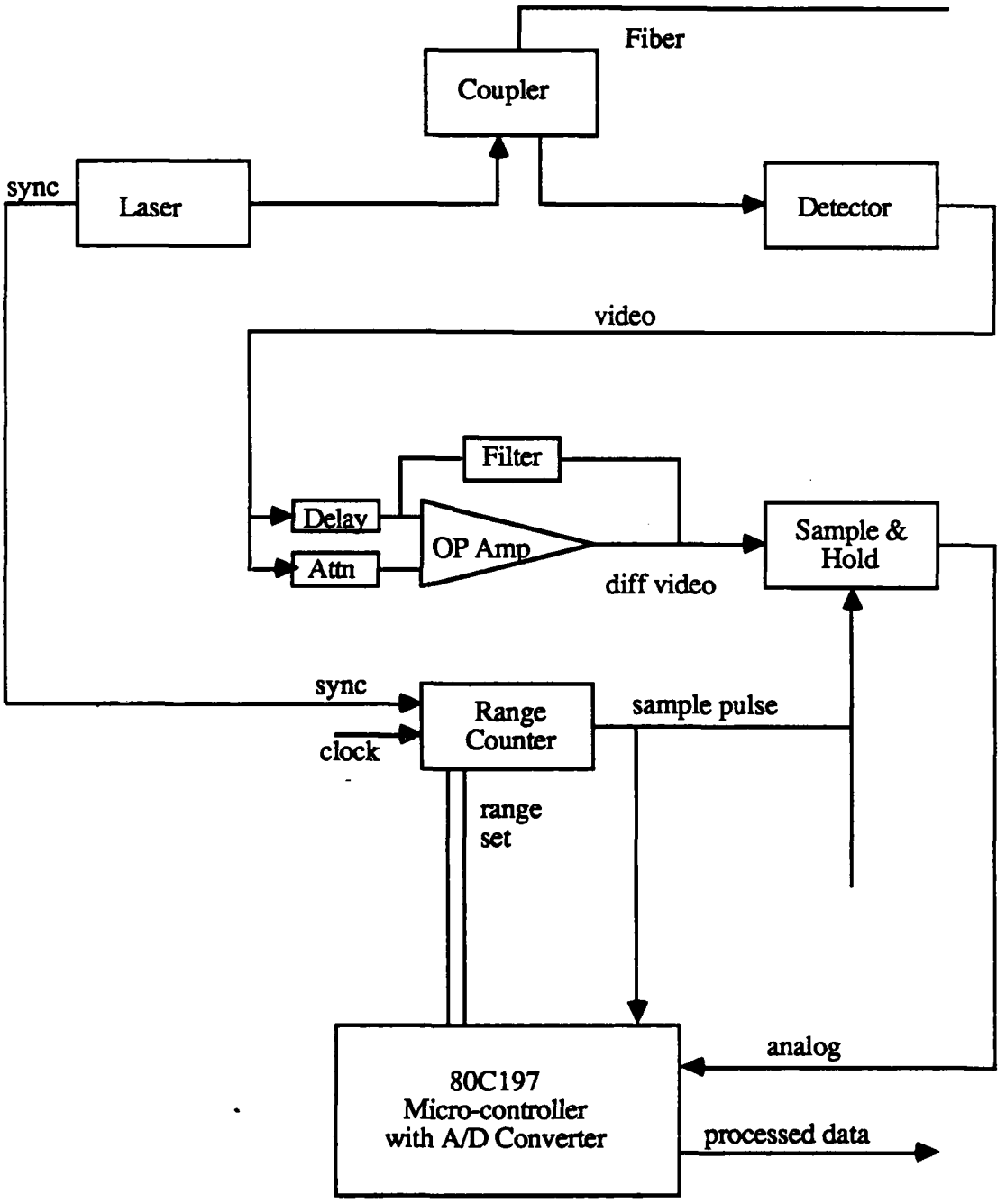

Figure 17 Custom OTDR strain sensing electronics

Typical values are:

Transducer spacing along fiber : 50-100 m.
Delay : 600-1200 nS.
Sampling rate (laser PRF) : 5000 Hz.

The OTDR section is emulated by a Laser Precision Corp. TD-9920 OTDR. The A/D and controller section is emulated by a PC with A/D card. Sampling rates for the entire structure are then nominally determined by the number of transducers N on the fiber, i.e., 5000 Hz/N.

As with the system currently in use consisting entirely of laboratory instrumentation, averaging would be performed to improve the signal-to-noise ratio. The sampling rate is then further reduced by the number of times M the samples are averaged, e.g., if four transducers are to be sampled and averaged 64 times, the highest sampling frequency for the structure is 5000/(4*64) = 19.53 Hz, which will satisfy the temporal sampling rate objectives we have set. As will be described shortly, even this sampling rate can be easily exceeded.

The total range achievable with our experimental setup is about 200 microstrains ($\partial L/L$). This number is derived by the total available dynamic range of the OTDR and the optical transmission of the fiber system - about 20 dB. This range may be used up by a single transducer, or it may be apportioned over several. This range is a function of the design of the transducer.

The following steps may be taken to increase this range:

1. Improve the coupling between the OTDR and the fiber. This would increase the range by about 25% by increasing the optical signal, and therefore improving the maximum signal-to-noise ratio of the system.
2. Use a better OTDR with a higher laser output and/or a lower receiver noise. An increase of at least 50% - 100% seems feasible based on evaluation of newer commercial OTDR instrumentation now available on the market.
3. Decrease the sensitivity of the transducers (by making them smaller). The tradeoff is direct, i.e., a reduction of the beam length of the transducer by a factor of two reduces sensitivity (and resolution) by the same factor, but doubles dynamic range. The sum of all signal drops across all transducers must remain the same (in this system ~20 dB),
4. Stagger the transducers on opposite sides of the beam. Bending the beam in one direction increases the signal step on one side but reduces it on the other. This doubles the net sensitivity, so that a reduction of the size of each transducer makes sense.

The transducers with a beam length of 5 cm (and microbend region of 2.5 cm) can detect a change of 1 microstrain provided the signal is filtered sufficiently. The raw signal-to-noise ratio is about 100 (i.e., the 20 dB referred to above). By averaging 100 sweeps this 1 microstrain change can be resolved. The linearity is also about +/- 1 microstrain.

To overcome the sampling rate limitations of the DP6000 sampling scope, a custom sampling circuit was designed. This circuit uses a delay line to develop a signal proportional to the signal drop across the transducers. Using a sample-and-hold circuit makes the timing uncritical. Samples may now be taken at the pulse rate of the OTDR (5 kHz); if a custom OTDR is used, this pulse rate can be increased to 100 kHz for a fiber sensor system up to 1 km in length. By using four sample-and-hold circuits, four transducers may be sampled at this rate. The resulting total sampling rate of 400 kHz is well within the

capabilities of currently available A/D converters. Requiring an averaging of 100 samples per measurement gives us an overall measurement rate of 4 kHz. This is a factor of 200 above the desired rate of 20 Hz, leaving room for circuit simplifications. Even using the present OTDR the 20 Hz rate can easily be met.

Figure 18 contains a photograph of the circuitry developed. It performs sample-and-hold for one transducer at the internal triggering rate of the OTDR - 5 kHz. Note from the oscilloscope trace in Figure 19 the signal slope is eliminated, which removes any signal error to jitter in the sampling trigger. The original OTDR wave form has a negative slope log-linear characteristic and the signal level is critically dependant on timing. The new sampling technique overcomes this dependance.

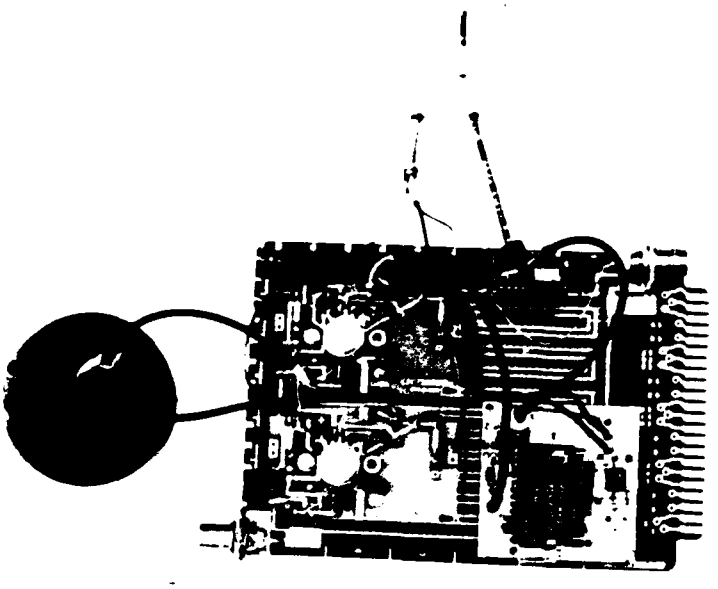

Figure 18 Photograph of sample-and-hold circuitry

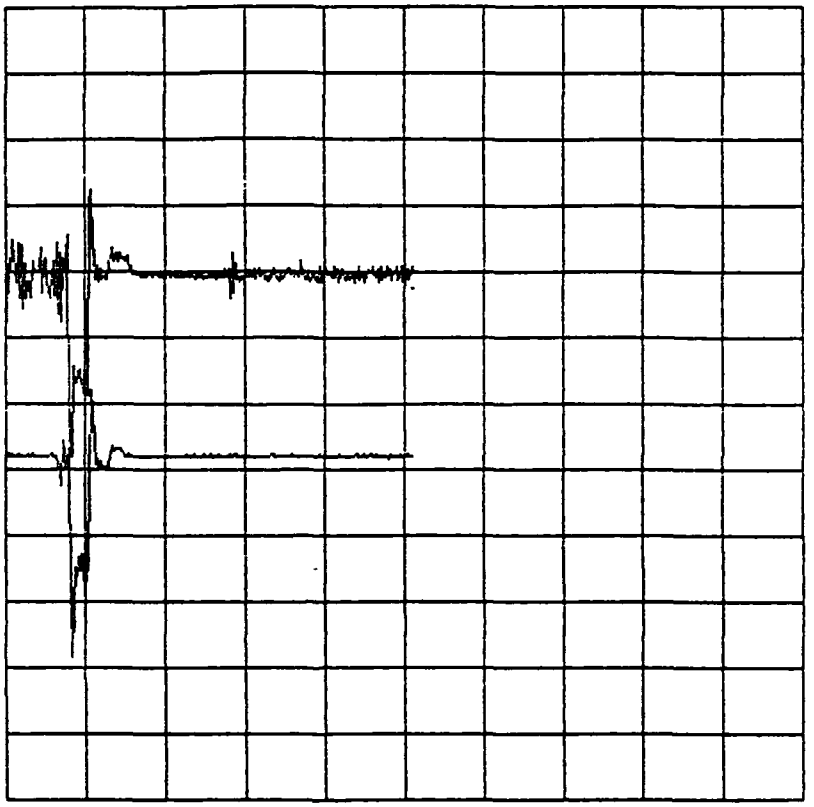

Horizontal scale:	4μsec/division
Vertical scale:	0.5 V/division
Upper trace:	analog signal
Lower trace:	sampled and digitized signal

Sensor signal is derived from anywhere on the flat portion of the trace. Averaging will improve signal-to-noise ratio. Resolution is limited by choice of A/D converter.

Figure 19 Digitized traces of output of sample-and-hold circuit

REAL-TIME DATA ACQUISITION

The advantages of the custom circuitry that has been implemented is apparent in the proof of concept for real-time data acquisition. For this purpose we describe one of the operational modes of the circuit: detection of strain from one transducer at acquisition rates sufficient to satisfy the objective of sampling strain at up to four locations at a 20 Hz update rate.

Figure 20 is a trace obtained and displayed in real-time from one transducer. The OTDR waveform is sampled at the full triggering rate of 5K waveforms per second. The sample-and-hold circuit detects and saves only the voltage shift occurring in the time interval which corresponds to the location of the transducer. This voltage is captured by an A/D interface card to a PC-AT compatible computer. 250 successive samples are sampled and averaged. Thus the signal is an average over a 0.05 sec interval, yielding an effective sampling rate of 20 Hz.

To maintain the same rate of sampling over a system of several transducers, the averaging per transducer must be reduced, e.g., four transducers can be sampled at 20 Hz if the averaging per transducer is reduced to 62 samples, with some degradation in signal-to-noise ratio. This rate is limited only if a single CPU is involved in the signal processing, which is the case here, in which a PC-AT system was used to capture the data. It is possible to parallelize the system by providing a sample-and-hold circuit and integrated A/D-microprocessor single chip computer for each transducer.

Another solution to overcoming the sampling and averaging bottleneck is to customize the OTDR with a higher trigger rate. The 5 kHz trigger rate is set for testing fibers up to 20 km in length. A 1 km fiber, more appropriate to the scope of this sensor, could be interrogated at up to 100 kHz rates. The sample-and hold circuitry described and demonstrated here can easily tolerate this sampling speed.

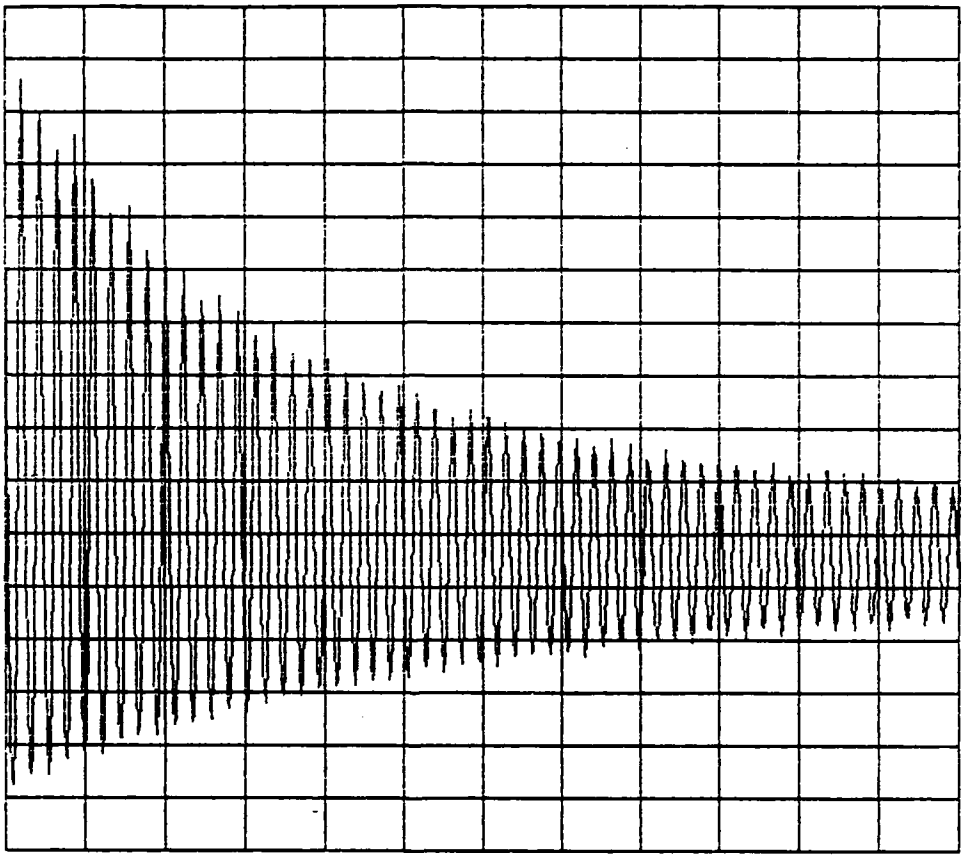

Horizontal scale: 2.5 seconds/division
Vertical scale: arbitrary (8-bit full scale resolution)

Figure 20 Real-time trace of strain signal acquired from OTDR sensor using one transducer. Sample-and-hold signal is averaged 250/sec and 20 data points are generated per second

SUMMARY

We have described an OTDR fiber optic microbend distributed sensor system which has demonstrated proof-of-concept performance using a single optical fiber and laboratory instrumentation as the goal of this program. We have developed a model for the strain developed by a cantilever mounted beam and the transduction of strain signal onto an optical fiber. The model has been encoded and enables us to generate a faithful reproduction of the beam shape for at least the fundamental and first overtone cantilever vibrational mode. The spatial deformation of the beam is the double integral of the strain map. Since the distributed strain is directly accessible from the multi-tapped nature of the single fiber, the beam shape can be reconstructed from the data, as has been shown for the fundamental mode.

Desirable characteristics such as dynamic range, sensitivity, dynamic sampling rates, power budget and permissible numbers of sensing sights which can be accessed through a single fiber have been analyzed. Resolution, as it pertains to the system demonstrated, is +/- 1 microstrain, but transducer design trade-offs have been identified which clearly indicate how higher resolution is possible. Dynamic range of the transducer is +/- 40 microstrains, but this too is dependant on transducer design, which is well understood. The signal to noise range for the system demonstrated is 20 dB with signal averaging, but improvements in lowering the detector noise level, increasing the laser output power, and reducing the coupling losses in fiber splices through selection of better couplers all indicate that a higher dynamic range is possible. Sampling rates in the primary demonstration system are limited to the digitization and re-arming rates of the digital oscilloscope: 2Hz. Entire waveforms are digitized from which the relevant data is extracted.

While proof of concept in the acquisition of strain data has been shown with the laboratory instrumentation system, real-time sensing and signal processing required the development of custom signal acquisition and processing hardware. The resulting custom system has demonstrated capability to sample at 5 kHz rates, but is theoretically suitable to 100 kHz with sensors distributed over a fiber up to 1 km in length. Using a single CPU, the product of the number of sensors and the number of samples averaged per transducer, divided into the OTDR trigger rate (e.g., 5 kHz of the system demonstrated, up to 100 kHz for a 1 km fiber) yields the maximum update rate available to produce a distributed strain map. There appears to be no restraint on sensing modal vibrations in large space structures up to 10 Hz, which requires that the sampling be at least above the Nyquist frequency (20 Hz) and preferably higher.

REFERENCES

1. Schoenwald, J. S. and P. M. Beckham, P. M. Distributed Fiber-Optic Sensor for Passive and Active Stabilization of Large Structures, Rev. of Prog. QNDE, Ed. Thompson, D. O. and Chimenti, D. E. Plenum: New York, pp. 568-573, 1988.

2. Asawa, C. K., Yao, S. K., Stearns, R. C., Mota, N. L. and Downs, J. W., "High-sensitivity fibre-optic strain sensors for measuring structural distortion," Electronics Letter

3. J. E. Midwinter, Optical Fibers for Transmission, John Wiley: New York, pp. 389-393, 1979.

4. Herga, Inc., West Chester PA 19380.